

# Dalton Transactions

Accepted Manuscript



This is an *Accepted Manuscript*, which has been through the Royal Society of Chemistry peer review process and has been accepted for publication.

*Accepted Manuscripts* are published online shortly after acceptance, before technical editing, formatting and proof reading. Using this free service, authors can make their results available to the community, in citable form, before we publish the edited article. We will replace this *Accepted Manuscript* with the edited and formatted *Advance Article* as soon as it is available.

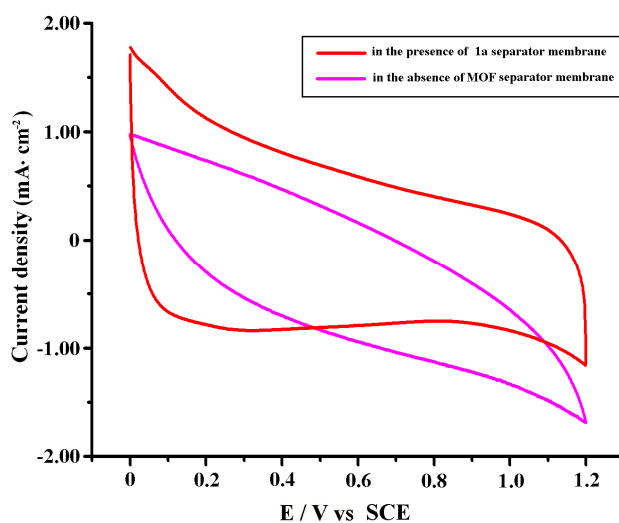
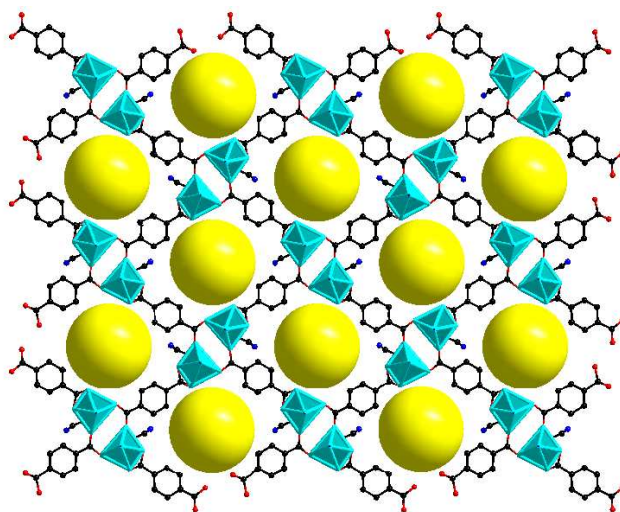
You can find more information about *Accepted Manuscripts* in the [Information for Authors](#).

Please note that technical editing may introduce minor changes to the text and/or graphics, which may alter content. The journal's standard [Terms & Conditions](#) and the [Ethical guidelines](#) still apply. In no event shall the Royal Society of Chemistry be held responsible for any errors or omissions in this *Accepted Manuscript* or any consequences arising from the use of any information it contains.

## Metal-Organic Frameworks Based on Rigid Ligands as Separator Membranes in Supercapacitor

Jiang-Ping Meng, Yun Gong,<sup>\*</sup> Qiang Lin, Miao-Miao Zhang, Pan Zhang, Hui-Fang Shi and Jian-Hua Lin<sup>\*</sup>

Two MOFs are used as the separator membranes in supercapacitor, after the charge-discharge experiment, the separator membrane of the Co compound becomes more porous.



# Metal-Organic Frameworks Based on Rigid Ligands as Separator Membranes in Supercapacitor

Jiang-Ping Meng,<sup>a</sup> Yun Gong,<sup>\*a</sup> Qiang Lin,<sup>a</sup> Miao-Miao Zhang,<sup>a</sup> Pan Zhang,<sup>a</sup> Hui-Fang Shi<sup>a</sup> and Jian-Hua Lin<sup>\*a,b</sup>

<sup>a</sup>Department of Applied Chemistry, College of Chemistry and Chemical Engineering, Chongqing University, Chongqing 400030, P. R. China Tel: +86-023-65106150 E-mail: gongyun7211@cqu.edu.cn

<sup>b</sup>Zhejiang University, Hangzhou 310058, P. R. China Tel: +86-0571-88981583 E-mail: jhlin@zju.edu.cn; jhlin@cqu.edu.cn; jhlin@pku.edu.cn

*This submission was created using the RSC Article Template (DO NOT DELETE THIS TEXT)  
(LINE INCLUDED FOR SPACING ONLY - DO NOT DELETE THIS TEXT)*

Two thermally stable MOFs formulated as CoL(1,4-bdc)·2DMF (L = 3, 5- bis (5- (pyridin-4-yl)-4H-1,2,4-triazol-3-yl)pyridine), 1,4-H<sub>2</sub>bdc = 1,4- benzenedicarboxylic acid) (**1**) and CdL(4,4'-bpc)·3DMF (4,4'-H<sub>2</sub>bpc = 4,4'-biphenyldicarboxylic acid) (**2**) have been solvothermally synthesized and they exhibit a similar uninodal 6-connected 3D architecture with {4<sup>12</sup>.6<sup>3</sup>}-pcu topology. MOF **1** shows a non-interpenetrated network with larger channel, whereas MOF **2** exhibits a 3-folded interpenetrating framework with smaller pore size. When the two MOFs are used as the separator membranes in supercapacitor, the equivalent series resistance (R<sub>es</sub>) is larger than the R<sub>es</sub> in the blank supercapacitor, and the less the current density, the more the R<sub>es</sub>. After charged and discharged at the low current density, the supercapacitor with the separator membrane of MOF **1** (denoted as **1a**) possesses a much larger specific capacitance (SC) than the blank supercapacitor, and the amorphous separator membrane **1a** shows a more porous morphology than the original MOF membrane **1**.

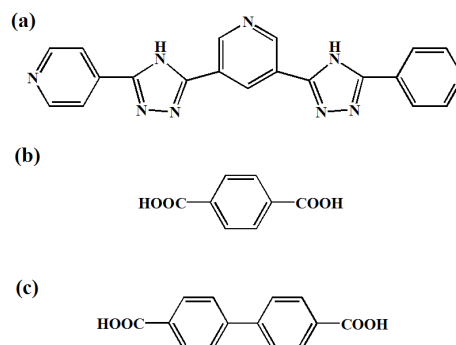
## Introduction

Recently, porous materials including metal-organic frameworks (MOFs) or coordination polymers composed of metal ions/clusters and coordinated linkers are one of the most rapidly growing categories of materials.<sup>1</sup> Owing to their fascinating structures and unusual properties such as permanent porosity, high surface area, good thermostability, and uniformly-structured cavities, MOFs have many applications, including gas adsorption/storage, separation, catalysis, adsorption of organic molecules, drug delivery and carriers for nanomaterials.<sup>1</sup> MOFs, as a replacement of the protonconducting membrane, have also been receiving great attention.<sup>2-4</sup> However, the ion transport behaviors in the channels of MOFs are scarcely reported.<sup>5</sup>

With the depletion of fossil fuels, supercapacitor, as one kind of typical electrochemical energy storage device, has received tremendous attention due to their faster and higher power capability, long life, wide thermal operating range compared with secondary batteries.<sup>6</sup> Generally, supercapacitors are composed of two electrodes separated by a dielectric porous membrane, impregnated by an electrolyte. The functions of the separator membranes are avoiding short circuits between two electrodes, and allowing the desired ions to pass through without much difficulty.

In an attempt to investigate the ion transport behaviors through MOFs, our strategy is to utilize MOF as the separator membrane in supercapacitor and investigate the effect of the MOF-based separator membrane on the electrochemical property of supercapacitor. In the present work, a rigid N-donor, 3,5-bis(5-(pyridin-4-yl)-4H-1,2,4-triazol-3-yl) pyridine (**L**) was synthesized.<sup>7</sup> Based on **L** and rigid dicarboxylate coligands, 1,4-benzenedicarboxylic acid (**1,4-H<sub>2</sub>bdc**) and 4,4'-biphenyldicarboxylic acid (**4,4'-H<sub>2</sub>bpc**) (Scheme 1), two thermally stable MOFs formulated as CoL(1,4-bdc)·2DMF (**1**) CdL(4,4'-bpc)·3DMF (**2**) were solvothermally synthesized in

moderate yields. Their thermal stabilities, gas sorption and their effects on the electrochemical behaviors of supercapacitor have been investigated.



**Scheme 1** Schematic representation of **L** (**a**), 1,4-H<sub>2</sub>bdc (**b**) and 4,4'-H<sub>2</sub>bpc (**c**).

## Experimental

**General Considerations** All chemicals purchased were of reagent grade and used without further purification. Graphene was purchased from Nanjing XFNANO Materials Tech Co., Ltd. Qualitative filter paper (medium speed) is from Hanzhou paper Co., Ltd. The melting point was determined using an uncorrected X-4 melting point apparatus of Beijing Kaifu Company. C, H, N elemental analyses were performed on an Elementar Vario MICRO E III analyzer. IR spectra were recorded as KBr pellets on a Nicolet iS50 FT-IR spectrometer. The powder XRD (PXRD) data were collected on a RIGAKU DMAX2500PC diffractometer using Cu K $\alpha$  radiation. TGA was performed on a NETZSCH STA 449C thermogravimetric analyzer in flowing N<sub>2</sub> with a heating rate of 10°C·min<sup>-1</sup>. The

gas sorption isotherms were measured using a Quadrasorb ZSI-MP-21 volumetric gas adsorption instrument. A 769YP-24B powder pelletizer of Tianjin Keqi Company was used for the preparation of the MOF separator membrane. The morphologies of the samples were observed by scanning electron microscopy (SEM, JSM-7600F, JEOL). Raman spectra were conducted on a Nicolet iS50 Raman spectrometer.

**Electrochemical measurements** The electrochemical measurements were done in a three-electrode test cell with a saturated calomel electrode (SCE) and a platinum foil as the reference and counter electrode, respectively. 4 mg solid sample was ultrasonicated in a mixture of acetone (1 mL) and nafion (0.05 mL) solution, then was deposited on a glassy carbon electrode with a 0.2 cm<sup>2</sup> of the electroactive area to obtain the working electrode after the solvent is dried by an IR lamp. The electrodes were immersed in a N<sub>2</sub> degassed NaNO<sub>3</sub> (0.05 M, 50 mL) aqueous solution and a CHI660E electrochemical workstation was used in the electrochemical measurements. Electrochemical impedance spectroscopy (EIS) measurements were conducted in the range of 0.01 Hz - 1 MHz. The galvanostatic charge/discharge measurements were conducted on a Neware BTS-5V5mA battery analyzer.

**Synthesis of L:** L was prepared according to the literature method.<sup>7</sup> Melting point: >250 °C. IR (cm<sup>-1</sup>): 3399(m), 3044(m), 2681(m), 1865(w), 1614(s), 1576(s), 1454(s), 1426(m), 1371(s), 1312(w), 1221(w), 1162(m), 1142(m), 1018(s), 976(s), 905(w), 835(m), 752(m), 698(m), 525(w)..

**Synthesis of CoL(1,4-bdc)·2DMF (1):** A mixture of Co(NO<sub>3</sub>)<sub>2</sub>·6H<sub>2</sub>O (0.025 mmol, 0.007 g), L (0.0125 mmol, 0.005 g), 1,4-H<sub>2</sub>bdc (0.0125 mmol, 0.002 g) and DMF (8 mL) was sealed in a Teflon-lined autoclave and heated at 150 °C for 3 days, then followed by slow cooling to room temperature. The resulting red block crystals were filtered off (yield: ca. 72 % based on L). Elemental Anal. Found: C, 53.80; H, 4.25; N, 20.91 %. Calcd. For CoC<sub>33</sub>H<sub>31</sub>N<sub>11</sub>O<sub>6</sub>: C, 53.81; H, 4.24; N, 20.92 %. IR (cm<sup>-1</sup>): 3092(s), 2922(s), 1964(w), 1659(s), 1621(s), 1584(s), 1504(m), 1395(s), 1138(m), 1096(m), 1016(m), 993(m), 974(m), 845(m), 804(m), 750(s), 708(m), 532(m).

**Synthesis of CdL(4,4'-bpc)·3DMF (2):** The synthesis of MOF 2 was carried out as described above for complex 1, but starting with the mixture of Cd(NO<sub>3</sub>)<sub>2</sub>·4H<sub>2</sub>O (0.0375 mmol, 0.012 g), L (0.0125 mmol, 0.005 g), 4,4'-H<sub>2</sub>bpc (0.0125 mmol, 0.003 g) and DMF (8 mL). The yield of the colorless block crystals is ca. 68 % based on L. Elemental Anal. Found: C, 53.72; H, 4.50; N, 17.88 %. Calcd. for CdC<sub>42</sub>H<sub>42</sub>N<sub>12</sub>O<sub>7</sub>: C, 53.71; H, 4.51; N, 17.89 %. IR (cm<sup>-1</sup>): 3427(s), 2924(m), 1657(s), 1618(s), 1584(s), 1530(m), 1393(s), 1142(w), 1097(m), 1046(w), 1016(w), 1007(w), 843(m), 772(m), 708(m), 528(w), 426(w).

**Preparation of the separator membranes of MOFs 1 and 2** The separator membrane of MOF 1 or 2 was prepared as follows: 10 mg desolvated powder of MOF 1 or 2 was immersed in the 0.05 M NaNO<sub>3</sub> aqueous solution overnight, then filtered and dried in oven at 80 °C for 2 h. The sample was pressed into a round slice with a diameter of 10 mm and a thickness of ca. 0.1 mm under the pressure of 20 MPa (Fig. S1a-b). And the SEM images of the separator membranes of MOFs 1 and 2 are shown

in Fig. S2. The supercapacitor was fabricated as shown in Fig. S3: Two Ni substrates were used as current collectors, and each piece of the collector was covered by 0.25 mg graphene as electrode material. The separator membrane of MOF 1 or 2 was sandwiched by two pieces of filter papers with two drops of the NaNO<sub>3</sub> aqueous solution on each side as the electrolyte. Here, the graphene was commercially purchased from Nanjing XFNANO Materials Tech Co., Ltd, which exhibits graphene's characteristic Raman signals at approximately 1342 cm<sup>-1</sup> (D peak), 1571 cm<sup>-1</sup> (G peak) and an overtone peak near 2682 cm<sup>-1</sup> (2D peak) (Fig. S4).<sup>8</sup> Before the cyclic voltammetry (CV) measurement, the fabricated supercapacitors were left to stand undisturbed overnight.

**X-ray crystallography** Single-crystal X-ray data for MOFs 1 and 2 were collected on a SuperNova diffractometer using graphite monochromated Mo Ka ( $\lambda = 0.71073 \text{ \AA}$ ) radiation at room temperature. Empirical absorption correction was applied. The structures were solved by direct methods and refined by the full-matrix least-squares methods on  $F^2$  using the SHELXTL-97 software.<sup>9</sup> All non-hydrogen atoms were refined anisotropically. All of the hydrogen atoms were placed in the calculated positions. The solvent molecule in MOF 1 was highly disordered and was impossible to refine using conventional discrete-atom models, thus the contribution of partial solvent electron densities were removed by the SQUEEZE routine in PLATON.<sup>10</sup> The final chemical formula of MOF 1 was estimated from the SQUEEZE result combined with the TGA result. The crystal data and structure refinements for MOFs 1 and 2 are summarized in Table 1. Selected bond lengths and angles for MOFs 1 and 2 are listed in Table S1 in the supporting information. The CCDC reference numbers are the following: 987758 for MOF 1 and 987759 for MOF 2.

**Table 1** Crystal data and structure refinements for MOFs 1 and 2

MOF	1	2
Empirical formula	CoC <sub>33</sub> H <sub>31</sub> N <sub>11</sub> O <sub>6</sub>	CdC <sub>42</sub> H <sub>42</sub> N <sub>12</sub> O <sub>7</sub>
<i>M</i>	736.61	939.28
Crystal system	orthorhombic	monoclinic
Space group	<i>Pcma</i>	<i>P2<sub>1</sub>/c</i>
<i>a</i> / Å	19.4254(7)	11.1597(5)
<i>b</i> / Å	21.878(2)	22.0750(9)
<i>c</i> / Å	15.5780(8)	17.4340(7)
$\alpha$ / °	90	90
$\beta$ / °	90	99.424(4)
$\gamma$ / °	90	90
<i>V</i> / Å <sup>3</sup>	6620.5(8)	4236.9(3)
<i>Z</i>	4	4
<i>D</i> <sub>calcd</sub> / g cm <sup>-3</sup>	0.592	1.472
$\mu$ / mm <sup>-1</sup>	0.280	0.581
No. of unique reflens	6003	7399
reflens used [ <i>I</i> > 2 $\sigma$ ( <i>I</i> )]	4012	5925
F(0 0 0)	1204	1928
Goodness-of-fit on $F^2$	1.073	1.133
Final <i>R</i> indices	<i>R</i> <sub>f</sub> = 0.0996, [ <i>I</i> > 2 $\sigma$ ( <i>I</i> )] <i>wR</i> <sub>f</sub> = 0.2818	<i>R</i> <sub>f</sub> = 0.0620, <i>wR</i> <sub>f</sub> = 0.1369
$R_f = \sum   F_o  -  F_c   / \sum  F_o $ ; $wR_f = \sum [w(F_o^2 - F_c^2)^2] / \sum [w(F_o^2)^2]^{1/2}$		

## Results and discussion

**Crystal Structure of CoL(1,4-bdc)·2DMF (1)** Single-crystal X-ray diffraction analysis reveals that MOF **1** crystallizes in the *orthorhombic* space group *Pcma* (**Table 1**). Its asymmetric unit contains one crystallographically independent Co(II) and one 1,4-bdc<sup>2-</sup> with 50% occupancy, half L, and one uncoordinated DMF molecule. Co(1) exhibits a distorted octahedral geometry, being defined by two pyridine N atoms from two L [Co-N 2.179(4) Å], four O atoms from one chelating carboxylate group and two bidentate bridging carboxylate groups from three 1,4-bdc<sup>2-</sup> [Co-O 1.933(5)-2.360(7) Å] (**Fig. 1a-b** and **Table S1**). One carboxylate group of the completely deprotonated 1,4-bdc<sup>2-</sup> exhibits a bidentate bridging mode, which links two Co(II) ions into a Co<sub>2</sub> unit (**Fig. 1a-b**). The 1,4-bdc<sup>2-</sup> ligand connects two Co<sub>2</sub> units with one bidentate bridging and one chelating carboxylate groups, thus it can be considered a 2-connected node and not counted as node topologically (**Fig. 1a-b**).<sup>11</sup> The crystallographically independent L is almost a planar molecule with 6.6 and 5.9 ° of the dihedral angles between the neighboring pyridine ring and triazol ring. L links two Co(II) ions via its two terminal pyridine N atoms, which also functions a 2-connected node (**Fig. 1a-b**).<sup>11</sup> In MOF **1**, the Co<sub>2</sub> unit connects six neighboring Co<sub>2</sub> units via four μ<sub>2</sub>-1,4-bdc<sup>2-</sup> ligand and two double strands of μ<sub>2</sub>-L ligands, thus it can be defined as a 6-connected node with a Schläfli symbol of (4<sup>12</sup>.6<sup>3</sup>) (**Fig. 1**).<sup>12</sup> Topological analysis using *TOPOS* software indicates MOF **1** exhibits a uninodal 6-connected non-interpenetrated three-dimensional (3D) architecture with {4<sup>12</sup>.6<sup>3</sup>}-*pcu* topology (**Fig. 1c**).<sup>12</sup>

The solvent-accessible volume of the unit cell of MOF **1** is 4563.3 Å<sup>3</sup>, which is approximately 68.9 % of the unit-cell volume (6620.5 Å<sup>3</sup>).<sup>13</sup> As show in **Fig. 1b**, MOF **1** exhibits a one-dimensional (1D) rectangular channel with a window size of ca. 7.8 × 9.1 Å<sup>2</sup>.

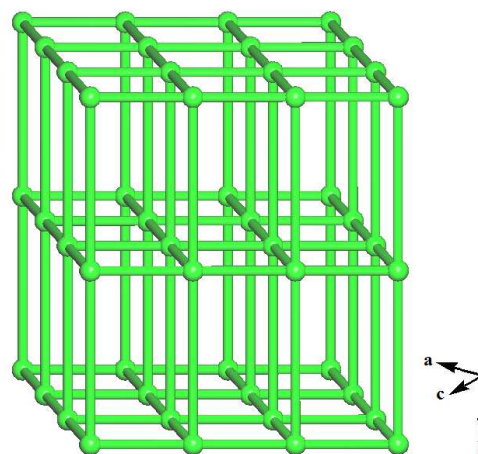
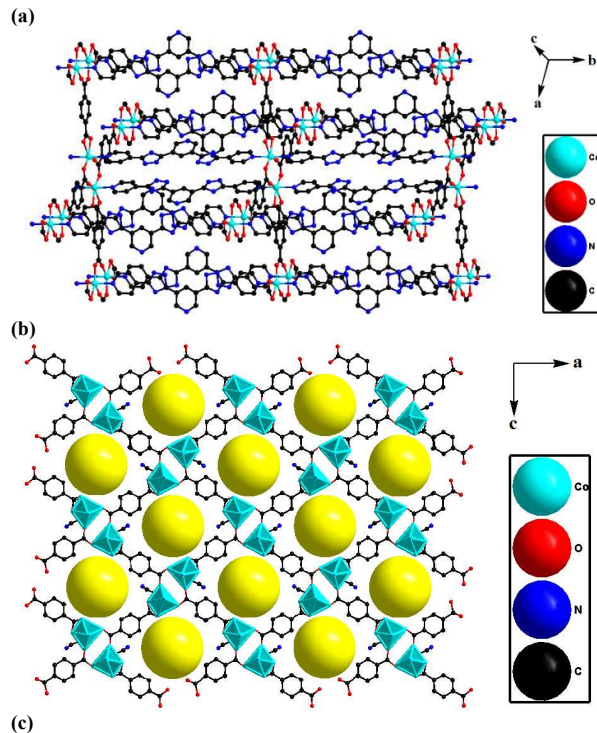


**Fig. 1** 3D architecture constructed by Co<sub>2</sub> unit, L and 1,4-bdc<sup>2-</sup> in MOF **1** (a); 1D channel viewed along *b*-axis in MOF **1** with the window size denoted as yellow ball (b) (H atoms omitted for clarity); Schematic illustrating the non-interpenetrated 3D framework with {4<sup>12</sup>.6<sup>3</sup>}-*pcu* topology in MOF **1** (c).

**Crystal Structure of CdL(4,4'-bpc)·3DMF (2)** In order to investigate the relationship between the ion transport behavior and the structure of MOF, another MOF formulated as CdL(4,4'-bpc)·3DMF (4,4'-H<sub>2</sub>bpc = 4,4'-biphenyldicarboxylic acid) (**2**) was solvothermally synthesized for comparison. MOF **2** crystallizes in the *monoclinic* space group *P2<sub>1</sub>/c* with one Cd(II), one 4,4'-bpc<sup>2-</sup>, one L and three uncoordinated DMF in the asymmetric unit (**Table 1**). Cd(1) in MOF **2** also shows a distorted octahedral geometry, being coordinated by two pyridine N atoms from two L [Cd-N 2.315(4)-2.326(4) Å] and four O atoms from three 4,4'-bpc<sup>2-</sup> [Cd-O 2.182(4)- 2.460(4) Å] (**Fig. 2a** and **Table S1**). The 4,4'-bpc<sup>2-</sup> displays a similar coordination mode to the 1,4-bdc<sup>2-</sup> in MOF **1** with a 39 ° of the dihedral angle between the two phenyl rings. Similar Cd<sub>2</sub> unit is observed in MOF **2**, and the 4,4'-bpc<sup>2-</sup> ligand connects two Cd<sub>2</sub> units with one bidentate bridging and one chelating carboxylate groups, it is considered a 2-connected node (**Fig. 2a**).<sup>11</sup> The L ligand links two Cd<sub>2</sub> units via its two terminal pyridine N atoms with 4.2-14.0 ° of the dihedral angles between the neighboring pyridine ring and triazol ring. Each Cd<sub>2</sub> unit connects six neighboring Cd<sub>2</sub> units via four μ<sub>2</sub>-4,4'-bpc<sup>2-</sup> and two double strands of μ<sub>2</sub>-L ligands, it is defined as 6-connected node (**Fig. 2b**).<sup>12</sup> MOF **2** also shows a similar uninodal 6-connected 3D framework with {4<sup>12</sup>.6<sup>3</sup>}-*pcu* topology (**Fig. 2b**).<sup>12</sup> However, because of the length of 4,4'-bpc<sup>2-</sup> longer than that of 1,4-bdc<sup>2-</sup>, MOF **2** shows 3-fold interpenetrated network (**Fig. 2b**).<sup>12</sup> And due to the entanglement, the solvent-accessible volume of the unit cell of MOF **2** is reduced to be 1712.1 Å<sup>3</sup>, which is approximately 40.4 % of the unit-cell volume (4236.9 Å<sup>3</sup>).<sup>13</sup> As show in **Fig. 2a**, 1D triangular channel with ca. 5.9 Å of height and ca. 9.7 Å of size length is observed in MOF **2**, which is smaller than the size of channel in MOF **1**.

(a)

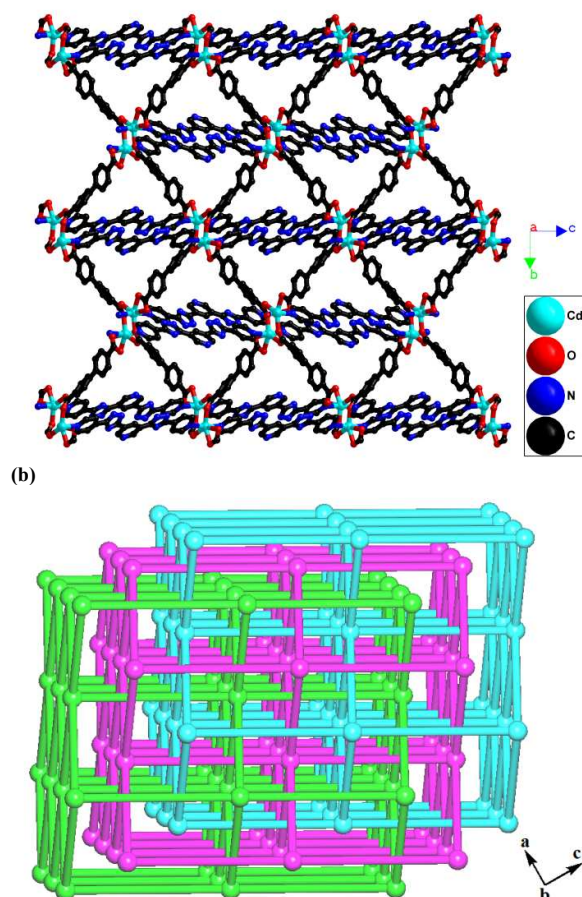


**Fig. 2** 3D architecture constructed by Cd<sub>2</sub> unit, L and 4,4'-bpc<sup>2</sup> in MOF 2 (H atoms omitted for clarity) (a); Schematic illustrating the 3-fold interpenetrated 3D framework with {4<sup>12</sup>.6<sup>3</sup>}-pcu topology in MOF 2 (b).

**Thermal stabilities of MOFs 1 and 2** Thermogravimetric analyses (TGAs) were carried out to examine the thermal stabilities of the two porous MOFs. The samples were heated up to 800 °C in N<sub>2</sub>. The TGA curve of MOF 1 reveals an initial weight loss of 19.8 % from 70 to 300 °C corresponding to the removal of two DMF molecules per formula unit (calcd. 19.6 %), resulting in the solvent free microporous framework, which starts decomposition at 390 °C (Fig. S5). MOF 1 was immersed in CH<sub>2</sub>Cl<sub>2</sub> and subjected to ultrasonic vibration for 4 h, and then evacuated at 300 °C in vacuum for 2 h. The powder XRD pattern of the desolvated MOF coincides with that simulated using the single-crystal data (Fig. S6a), which indicates that the porous host framework of the MOF is kept and MOF 1 possesses high thermal stability.

The TGA curve of MOF 2 show a one step weight loss between 30 and 240 °C corresponding to the loss of the uncoordinated solvent molecules (obsd. 23.3 %, calc. 23.4 wt%). The desolvated MOF 2 remained stable up to ~350 °C without any weight loss (Fig. S5). Similar desolvation method is applied for MOF 2, and the desolvated sample possesses its original host framework, as evidenced by the powder XRD patterns (Fig. S6b), indicating MOF 2 also possess good thermal stability.

**Sorption properties of MOFs 1 and 2** To confirm the porosities of MOFs 1 and 2, gas sorption experiments were

carried out. The N<sub>2</sub> sorption isotherm of the desolvated MOF 1 at 77 K reveals type I behavior typical for microporous materials with the Brunauer-Emmett-Teller (BET) surface area of 245 m<sup>2</sup>·g<sup>-1</sup> (Fig. 3). A plot of Horvath-Kawazoe (HK) differential pore volume indicates that MOF 1 contains pore of ca. 8.4 Å opening and pore volume of ca. 0.110 cm<sup>3</sup>·g<sup>-1</sup>, which is in agreement with the X-ray structural analysis. The desolvated MOF takes up 75.8 cm<sup>3</sup>·g<sup>-1</sup> nitrogen gas at 77K and 1 atm.

Based on the regular rectangular channel with a 8.4 Å of opening size in MOF 1 (Fig. 1b), which is larger than the diameters of the hydrated Na<sup>+</sup> (7.2 Å) and NO<sub>3</sub><sup>-</sup> (6.8 Å),<sup>14</sup> thus it is estimated that MOF 1 can act as a separator membrane for the ionic diffusion in supercapacitor when NaNO<sub>3</sub> is used as the electrolyte.

The sorption isotherm of N<sub>2</sub> for MOF 2 at 77 K also shows a type I behavior, but gives a BET surface area of 19 m<sup>2</sup>·g<sup>-1</sup> with pore of ca. 7.5 Å opening (Fig. 3). The pore volume is ca. 0.049 cm<sup>3</sup>·g<sup>-1</sup>, and the desolvated MOF 2 takes up 33.2 cm<sup>3</sup>·g<sup>-1</sup> nitrogen gas at 1 atm (Fig. 2). The result proves the size of channel in MOF 2 is smaller than that in MOF 1, which is in agreement with the X-ray structural analysis.

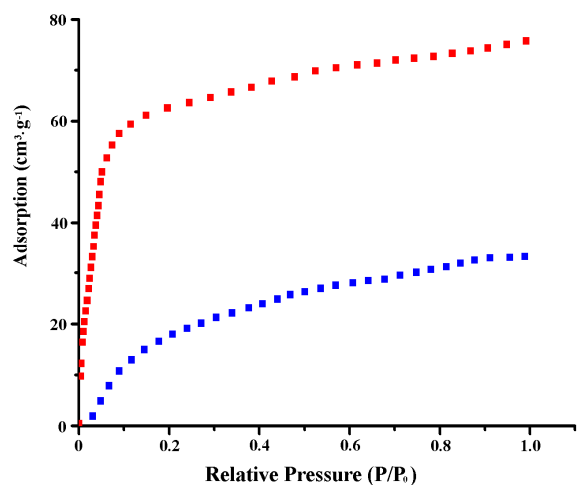


**Fig. 3** Adsorption isotherm of N<sub>2</sub> at 77 K for the desolvated MOFs 1 (red) and 2 (blue).

**Electrochemical properties of MOFs 1 and 2** The redox properties of MOFs 1 and 2 were evaluated by cyclic voltammetry (CV) experiments in a three-electrode cell with a saturated calomel electrode (SCE) and a platinum foil used as the reference and counter electrode, respectively. In a 0.05 M NaNO<sub>3</sub> aqueous solution (50 mL), it is found the CV of 4 mg MOF 1 modified-glassy carbon electrode (1-GCE) displays two irreversible reduction peaks at -0.80 and +1.02 V vs SCE in the potential range from -1.5 to 1.5 V vs SCE at a scan rate of 10 mV·s<sup>-1</sup> (Fig. 4 and Fig. S7a). The peak at -0.80 V vs SCE is similar to the reduction peak of -0.59 V at the 4 mg L modified-glassy carbon electrode (L-GCE) (Fig. 4, Fig. S7a and Fig. S7b), indicating it is probably associated with the reduction of the π electron from the ligand L.<sup>15</sup> However, the irreversible reduction peak at +1.02 V vs SCE is different from the redox waves at the bare glassy carbon electrode (GCE), L-GCE and 4 mg 1,4-H<sub>2</sub>bdc modified-glassy carbon electrodes (1,4-H<sub>2</sub>bdc-GCE), respectively (Fig. 4, Fig. S7 and Fig. S8), indicating it is probably ascribed to the redox of Co(II).<sup>15</sup>

CREATED USING THE RSC ARTICLE TEMPLATE - SEE WWW.RSC.ORG/ELECTRONICFILES FOR FURTHER DETAILS

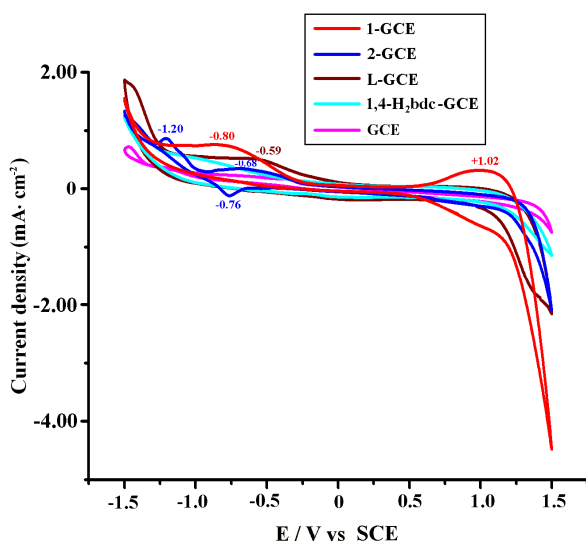


**Fig. 4** CVs of the bare GCE (pink), L-GCE (brown), 1,4-H<sub>2</sub>bdc-GCE (sapphire), 1-GCE (red) and 2-GCE (blue) in a 0.05 M NaNO<sub>3</sub> aqueous solution (50 mL) at a scan rate of 10 mV·s<sup>-1</sup>.

The CVs of 4 mg MOF 2 modified-glassy carbon electrode (2-GCE) in the similar NaNO<sub>3</sub> solution in the potential range of -1.5-1.5 V vs SCE are shown in Fig. 4 and Fig. S7d. The 2-GCE shows an irreversible reduction peak at -0.68 V vs SCE, which is similar to the irreversible reduction peak of -0.59 V vs SCE observed at the L-GCE (Fig. 4, Fig. S7b and Fig. S7d), indicating it is probably ascribed to the redox of the  $\pi$  electron from the ligand L.<sup>15</sup> And the 2-GCE displays a couple of quasi-reversible redox waves with cathodic peak ( $E_{pc}$ ) = +1.20 V vs SCE and anodic peak ( $E_{pa}$ ) = -0.76 V vs SCE, which are different from the redox waves at the bare GCE, L-GCE and 1,4-H<sub>2</sub>bdc-GCE, respectively (Fig. 4, Fig. S7 and Fig. S8), indicating it is probably ascribed to the redox of Cd(II).<sup>15</sup>

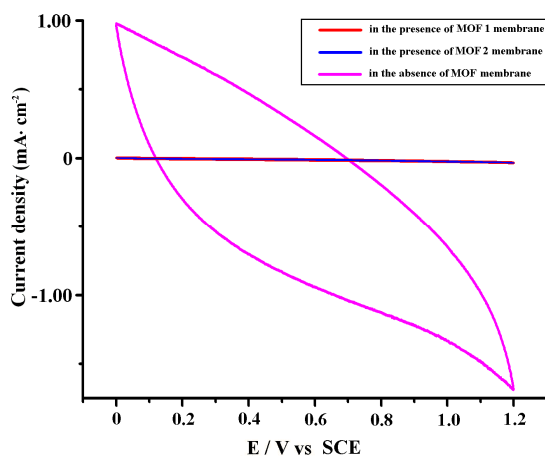


**Fig. 5** CVs of the supercapacitors in the absence and presence of the separator membrane of MOF 1 or 2 at a scan rate of 10 mV·s<sup>-1</sup>. Supporting electrolyte = 0.05 M NaNO<sub>3</sub> aqueous solution.

**CVs of the supercapacitor with or without the separator membranes of MOFs** In order to evaluate the ion transport behaviour through MOFs, MOFs 1 and 2 have been fabricated as separator membrane, and the electrochemical behaviors of the supercapacitors with and without the separator membrane of MOF have been evaluated by CV experiments. Herein, the

potential window is limited in the range of 0 ~ 1.2 V to avoid the electrolysis of water. As shown in Fig. 5 and Fig. S9a, in the absence of the separator membrane of MOF, at a scan rate of 10 mV·s<sup>-1</sup>, the CV exhibits an almost rectangular shape, suggesting its double-layer capacitive behavior. However, in the presence of the separator membrane of MOF 1 or 2, the area for the CV curve (Fig. 5 and Fig. S9b-c) almost can be neglectable in comparison with that in the absence of MOF (Fig. 5 and Fig. S9a), and the current in the blank supercapacitor (Fig. S9a) is approximately 300-400 times of that in the presence of MOF 1 or 2 (Fig. S9b-c), indicating the supercapacitor with the separator membrane of MOF 1 or 2 shows a much smaller specific capacitance (SC) in comparison to the blank supercapacitor, which is probably due to the large impedance from the separator membrane of MOF 1 or 2 because MOFs are usually not electroconductive.

**Galvanostatic charge-discharge experimental at high current density** The smaller SC in the presence of the separator membrane of MOF 1 is also proved by the galvanostatic charge-discharge plots of the supercapacitors, which is estimated from the discharge process. As shown in Fig. S10a-b, at a current density of 3.0 and 2.0 A·g<sup>-1</sup>, the discharge times ( $t_d$ ) in the presence of MOF 1 are ca. 2 s, which are much shorter than the 6 and 10 s of the discharge times in the blank supercapacitor (electrolyte: 0.05 M NaNO<sub>3</sub> aqueous solution) (Table S2). Furthermore, it is found the supercapacitor with the separator membrane of MOF 1 is easily to be overcharged and overdischarged in the potential window of 0~1.2 V (Fig. S10a-b), which is probably due to the microporous channel in MOF 1. When the charge-discharge cycles are performed at higher current density, there is not enough time for the ions to pass through the microporous channel. In an attempt to improve the ion transport behavior of the MOF-based separator membrane, the charge-discharge experiment had better be done at low current density.

**Galvanostatic charge-discharge experimental at low current density** The above expectation is evidenced by the charge-discharge experiment of the supercapacitor with the MOF 2-based separator membrane. As shown in Fig. S11a-b, at the low current density of 0.3 and 0.2 A·g<sup>-1</sup>, no overcharge or overdischarge is observed in the potential range of 0~1.2 V for the supercapacitor with the separator membrane of MOF 2 (electrolyte: 0.05 M NaNO<sub>3</sub> aqueous solution), and the discharge times are 8 and 16 s, respectively. However, for the blank supercapacitor without the MOF-based separator membrane, at the current density of 0.3 and 0.2 A·g<sup>-1</sup>, the galvanostatic charge-discharge curve shows much longer discharge time ( $t_d$  = 84 and 139 s, respectively) (Fig. 6a-b and Table S2), further indicating the blank supercapacitor possesses much larger SCs than that with the MOF-based separator membrane.

Based on the ohmic potential drops in the galvanostatic charge-discharge curve, it can be calculated the equivalent series resistance ( $R_{es}$ ) (see supporting information),<sup>16</sup> which is the sum of various resistances, including the electrolyte resistance ( $R_s$ ), separator membrane resistance ( $R_{sm}$ ) and the diffusion resistance ( $R_d$ ), etc. As shown in Table S2, it is found at the current density of 3.0, 2.0, 0.3 and 0.2 A·g<sup>-1</sup>, the  $R_{es}$  in the blank supercapacitor is 533, 630, 733 and 1000  $\Omega$ , respectively, indicating the less the current density, the more the  $R_{es}$ . As for the supercapacitor with

the separator membrane of MOF **2**, at the current density of 0.3 and 0.2 A·g<sup>-1</sup>, the  $R_{es}$  is 5300 and 6500 Ω, respectively (Table S2), which is larger than the  $R_{es}$  in the blank supercapacitor, further proves that the MOFs are not electroconductive.

In order to investigate the electrochemical stability of MOF **2**, the sample left on the 2-GCE after the CV experiment (denoted as **2a**) and the separator membrane of MOF **2** after the charge-discharge continuously for 100 cycles (denoted as **2b**) have been characterized by powder X-ray diffraction (PXRD). As shown in Fig. S6b, **2a** and **2b** exhibit PXRD patterns similar to that of MOF **2**, indicating MOF **2** is stable under the electrochemical condition, which is probably associated with the quasi-reversible redox property of the MOF. It also can be found that the PXRD of **2b** shows a significant amorphous hump, indicating the crystal sample utilized for the separator membrane lost its crystallinity to some extent after the charge-discharge experiments (Fig. S6b). It is evidenced by the SEM images of **2b**, as shown in Fig. S2g-h, in which two kinds of morphologies, nanowire and bulk powder are observed.

(a)

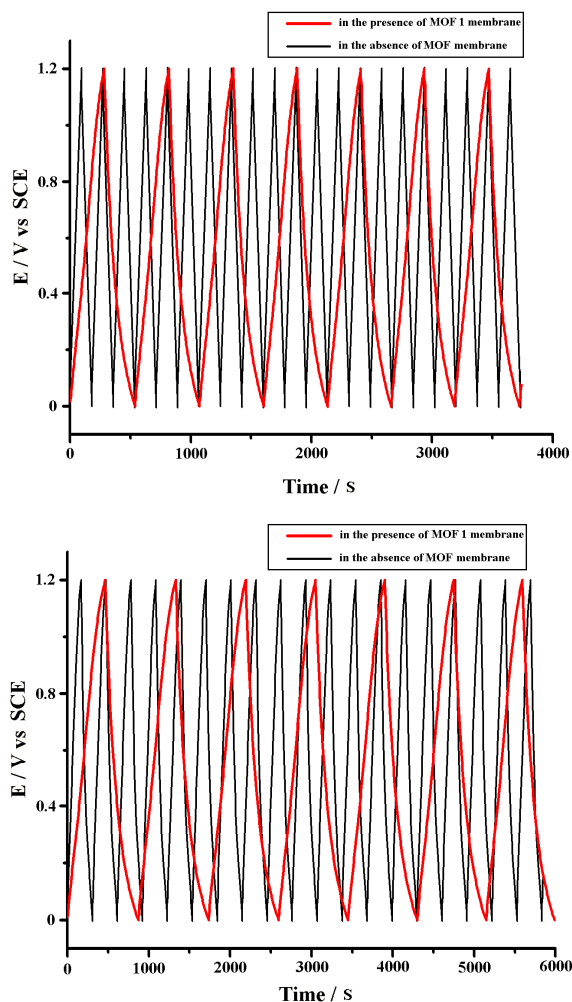


**Fig. 6** Typical charge-discharge cycles obtained in the absence (black) and presence of the separator membrane of MOF **1** (red) at 0.3 A·g<sup>-1</sup> (a) and 0.2 A·g<sup>-1</sup> (b), respectively. Supporting electrolyte = 0.05 M NaNO<sub>3</sub> aqueous solution.

In the present work, the charge-discharge experiment of the supercapacitor with the separator membrane of MOF **1** is also performed at the low current density of 0.3 and 0.2 A·g<sup>-1</sup> (electrolyte: 0.05 M NaNO<sub>3</sub> aqueous solution). As the red curves shown in Fig. 6a, the galvanostatic charge-discharge curve of the supercapacitor with the separator membrane of MOF **1** shows a almost ideal triangular shape in the potential range of 0~1.2 V at the current density of 0.3 A·g<sup>-1</sup>. However, the charge ( $t_c$ ) and discharge time ( $t_d$ ) is 270 and 260 s, respectively, indicating a 96 % of the energy deliverable efficiency ( $\eta$ ) (Fig. 6a and Table S2). And the 260 s of the discharge time is much longer than the 84 s of the discharge time in the blank supercapacitor without the MOF-based separator membrane, indicating the supercapacitor with **1**-based separator membrane possesses a 65 F·g<sup>-1</sup> of the SC, which is much larger than that in the blank supercapacitor (21 F·g<sup>-1</sup>) (Table S2). And at the current density of 0.2 A·g<sup>-1</sup>, the charge and discharge time is 445 and 400 s, indicating a 90 % of the energy deliverable efficiency ( $\eta$ ) and a 66.7 F·g<sup>-1</sup> of the SC (Fig. 6b and Table S2). And the 66.7 F·g<sup>-1</sup> of the SC is also larger than the 23.2 F·g<sup>-1</sup> in the blank supercapacitor.

As the red curves shown in Fig. 6, at the current density of 0.3 and 0.2 A·g<sup>-1</sup>, the  $R_{es}$  in the supercapacitor based on the separator membrane of MOF **1** is 1133 and 2000 Ω, respectively, which is larger than the 733 and 1000 Ω of the  $R_{es}$  in the blank system, which further proves the insulativity of the MOF.

**CVs of the supercapacitor with MOF 1-based separator membrane after the charge-discharge experiment** After the galvanostatic charge-discharge experiments at low current densities, the supercapacitor with the MOF **1**-based separator membrane was evaluated by CV measurement in the potential range of 0~1.2 V again. As shown in Fig. 7 and Fig. S12, it is found the CV area for the supercapacitor based on the MOF **1** separator membrane after charge-discharge at low current density is larger than that in the blank system, which is completely different from the phenomenon observed for the original supercapacitor before the charge-discharge experiment (Fig. 5). It is expected when charge and discharge at low current density, there is enough time for the ions to pass through the microporous channel, which will change the morphology and structure of the separator membrane of MOF **1**. The separator membrane of MOF **1** after the charge-discharge continuously for 100 cycles at low current density (denoted as **1a**) has been characterized by PXRD. However, after the charge-discharge experiment at low current density, **1a** is amorphous, as shown in Fig. S6a. As we know, amorphization is usual in inorganic materials and porous aromatic frameworks, and thermal or pressure-induced amorphization has been observed for MOFs. It is previously reported that the ion transporting capacity of crystalline MOFs might be improved during partial structural collapse.<sup>17</sup> Herein, the morphology of the separator membrane of MOF **1** before and after the charge-discharge experiment is characterized by SEM images, as shown in Fig. S2. It is found that the amorphous **1a** shows a more porous morphology than MOF **1**, then the ion transport behavior through the separator membrane is improved. The IR spectra of **1** and **1a** are shown in Fig. S13. It is found the characteristic bands of carboxylate groups in the range 1300~1700 cm<sup>-1</sup> are a bit different in the IR spectra of **1** and **1a**, indicating the structure of **1a** is different from that of MOF **1** (Fig. S13). As we known, cobalt oxide is a good supercapacitor electrode material,<sup>18</sup> which can produce



Faradaic redox current and improve the SC of supercapacitor. It is expected that cobalt oxide is probably obtained during the charge-discharge cycles, and the improved SC of the supercapacitor with the **1a** separator membrane is due to the Faradaic redox current that cobalt oxide in the separator membrane produces.

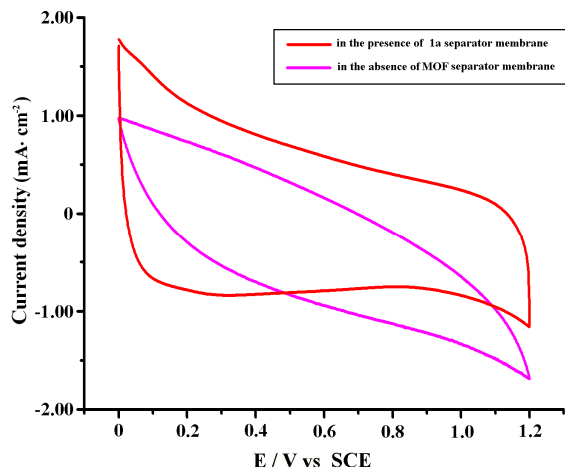


**Fig. 7** CVs of the supercapacitors in the absence and presence of the separator membrane of **1a** at a scan rate of  $10 \text{ mV}\cdot\text{s}^{-1}$ . Supporting electrolyte =  $0.05 \text{ M NaNO}_3$  aqueous solution.

Similar phenomena are observed when  $0.05 \text{ M}$  phosphate buffer aqueous solution ( $\text{pH } 6.8$ ,  $\text{H}_3\text{PO}_4/\text{NaOH}$ ) was used as the electrolyte instead of  $\text{NaNO}_3$  in the supercapacitor. As shown in **Fig. 8** and **Fig. S14**, it is found that the area for the CV curve with the **1a** separator membrane is also larger than that in the blank system, indicating the supercapacitor with **1a** membrane shows a larger SC than the blank system. The example further proves charge-discharge at low current density will improve the SC of the **1a**-based supercapacitor.

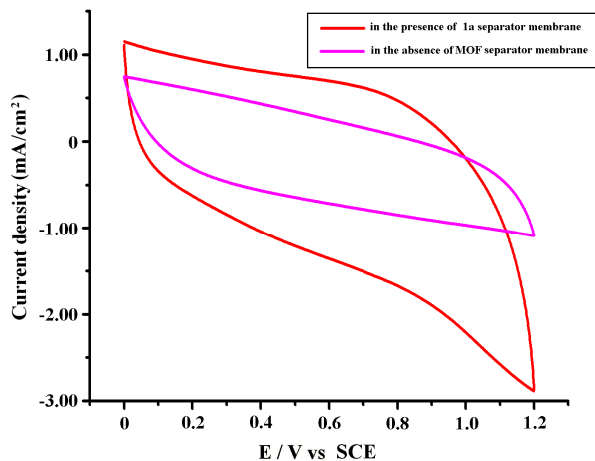


**Fig. 8** CVs of the supercapacitors in the absence and presence of the separator membrane of **1a** at a scan rate of  $10 \text{ mV}\cdot\text{s}^{-1}$ . Supporting electrolyte =  $0.05 \text{ M}$  phosphate buffer aqueous solution ( $\text{pH } 6.8$ ,  $\text{H}_3\text{PO}_4/\text{NaOH}$ ).

**EIS of the supercapacitor** In order to investigate why the supercapacitor with the **1a** separator membrane possesses the

larger SC than the blank supercapacitor, the electrochemical impedance spectroscopy (EIS) of the supercapacitor was measured. As shown in the Bode plots (**Fig. 9**), the  $R_s$  (electrolyte resistance) and the sum of  $R_s$  and  $R_{ct}$  (charge-transfer resistance) can be observed from the magnitude plot in the high and low frequency regions, respectively.<sup>15,19</sup> As shown in **Fig. 9**, herein, the sequences of either the  $R_s$  and  $R_{ct}$  are as follows: in the presence of **1a** < in the blank system < in the presence of **1**. It is indicating that either the  $R_s$  or the sum of  $R_s$  and  $R_{ct}$  in the presence of MOF-based separator membrane are greatly decreased by the charge-discharge experiment at the low current density. In other words, after the charge-discharge cycles, the electrolyte (ion) diffusion and the charge-transfer process within the supercapacitor based on the **1a** separator membrane are promoted.

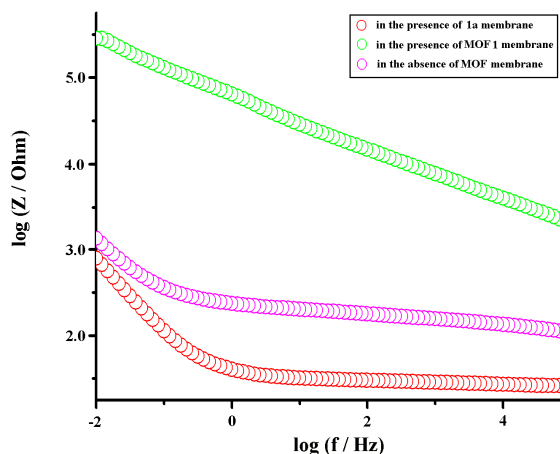


**Fig. 9** Bode plots ( $\log$  of impedance magnitude vs.  $\log f$ ) the supercapacitors at the initial potential of  $0 \text{ V}$  in the absence and presence of the separator membrane of MOF **1** before and after the charge-discharge experiment at the low current density. Supporting electrolyte =  $0.05 \text{ M NaNO}_3$  aqueous solution.

As discussed above, after the charge-discharge experiment at low current density, the separator membrane of MOF **1** become amorphous, which shows a more porous morphology than the original crystalline MOF. The improvement of the ion diffusion is probably associated with the more porous morphology of the **1a** separator membrane. The structure of the amorphous separator membrane **1a** is expected to be different from that of the original crystalline MOF **1** due to the irreversible redox peak of  $\text{Co(II)}$  in the CV of MOF **1** (**Fig. 4** and **Fig. S7a**). Since cobalt oxide is a good supercapacitor electrode material,<sup>18</sup> which can produce Faradaic redox current and improve the SC of supercapacitor, it is expected that cobalt oxide is probably obtained during the charge-discharge cycles. The promotion of the charge transfer by the amorphous separator membrane **1a** is probably associated with cobalt oxide in the separator membrane.

In order to prove the above expectation, another  $\text{Co(II)}$  MOF with good thermal stability formulated as  $\text{CoL}(4,4'\text{-bpc})\cdot 2\text{DMF}$  (**3**) was synthesized (see **ESI**, CCDC: 1044074). Single-crystal X-ray diffraction analyses reveal that the compositions of the  $\text{Co(II)}$  MOF **3** and the  $\text{Cd(II)}$  MOF **2** are similar except for different metal(II) ions in the structures. The solvent-accessible

volume of the unit cell of MOF **3** is  $1586.2 \text{ \AA}^3$ , which is approximately 39.0 % of the unit-cell volume ( $4070.7 \text{ \AA}^3$ ).<sup>13</sup>

As shown in **Fig. S15**, in a 0.05 M  $\text{NaNO}_3$  aqueous solution, 4 mg MOF **3** modified-glassy carbon electrode (**3-GCE**) displays two irreversible reduction peaks at  $-0.60$  and  $+1.10$  V vs SCE in the potential range from  $-1.5$  to  $1.5$  V vs SCE at  $10 \text{ mV}\cdot\text{s}^{-1}$  in a similar three-electrode cell. The electrochemical response at **3-GCE** (**Fig. S15** and **Fig. S16**) is similar to that observed at **1-GCE** (**Fig. 4** and **Fig. S7a**), indicating though the Co(II) MOFs **1** and **3** possess different structures, they show similar electrochemical property.

MOF **3** has been fabricated as the separator membrane of a supercapacitor in a similar method and the supercapacitor has been charged and discharged continuously for 100 cycles at low current density ( $0.3 \text{ A}\cdot\text{g}^{-1}$ ). The solid sample left on the **3-GCE** after the CV measurement (denoted as **3a**) and the separator membrane of MOF **3** after the charge-discharge experiment (denoted as **3b**) have been characterized by PXRD. As shown in **Fig. S6c**, both **3a** and **3b** are amorphous. CV and EIS of the supercapacitor with the **3b** separator membrane were also measured. Similarly, it is found that the CV area of the supercapacitor in the presence of **3b** is larger than that in the blank system without the **3b** separator membrane (**Fig. S17** and **Fig. S18**). And the  $R_s$  or the sum of  $R_s$  and  $R_{ct}$  in the presence of **3b** are lower than those in the blank system (**Fig. S19**). It is further expected that cobalt oxide was probably obtained after the separator membrane of MOF **3** was charged and discharged at low current density. And the improved CV area with respect to the blank supercapacitor is probably due to the Faradaic redox current that cobalt oxide in the separator membrane produces. The detailed mechanism is underway.

## Conclusion

In conclusion, two thermally stable MOFs formulated as  $\text{CoL}(1,4\text{-bdc})\cdot 2\text{DMF}$  (**1**) and  $\text{CdL}(4,4'\text{-bpc})\cdot 3\text{DMF}$  (**2**) have been solvothermally synthesized and structurally characterized by single-crystal X-ray diffraction. The two MOFs exhibit a similar uninodal 6-connected 3D architecture with  $\{4^{12}.6^3\}$ -pcu topology. MOF **1** shows a non-interpenetrated network with larger channel, whereas 3-folded interpenetration and much smaller pore size are observed in MOF **2**. And the porosities of the two MOFs are proved by the  $\text{N}_2$  sorption experiments. When the two MOFs are used as the separator membranes in supercapacitor, at the same current density, the  $R_{es}$  in the supercapacitor is larger than the  $R_{es}$  in the blank supercapacitor, which is due to the insulativity of MOFs. And the less the current density, the more the  $R_{es}$ .

When charged and discharged at higher current density, the supercapacitor with the separator membrane of MOF **1** or **2** possesses a much smaller SC than the blank supercapacitor, which is associated with the insulativity of MOFs. However, after charged and discharged at the low current density, the supercapacitor based on the **1a** separator membrane possesses a much larger SC than the blank supercapacitor, and the EIS results indicate the electrolyte (ion) diffusion and the charge-transfer process within the supercapacitor based on the **1a** separator membrane are promoted. The improvement of the ion transporting capacity of the separator membrane is associated with the more porous morphology after the charge-discharge experiment at low current density. It is expected that cobalt

oxide is probably obtained during the charge-discharge cycles at low current density, and the improved SC of the supercapacitor with the **1a** separator membrane is probably due to the Faradaic redox current that cobalt oxide in the separator membrane produces. The detailed mechanism is underway.

In the present work, MOF **2** is stable under the electrochemical condition, and the separator membrane of the crystalline MOF **2** lost its crystallinity to some extent after the charge-discharge experiments. And the supercapacitor with the separator membrane of MOF **2** shows a much lower SC than that with the **1a** separator membrane. After the charge-discharge cycles at low current density, the amorphous separator membrane **1a** shows a porous morphology (**Fig. S6c-d**), but **2** shows nonporous nanowire and nonporous powder (**Fig. S6g-h**). And due to the different metal (II) ions in the frameworks, the electrochemical stabilities of the two MOFs are different. The detailed mechanism is underway.

## Supporting Information

Crystallographic data; TG curve; PXRD patterns; CVs; SEM images; Raman spectra; Charge-discharge plots; Supercapacitive data; IR spectra and other supplementary material are included in the supporting information. This information is available free of charge via the Internet at <http://pubs.rsc.org/>.

Financial supports from the National Natural Science Foundation of China (No. 21371184), the Fundamental Research Funds for the Central Universities (No. CQDXWL-2012-024), the large-scale instrument and equipment open foundation in Chongqing University (No. 201406150041), and Chongqing Key Laboratory of Chemical Process for Clean Energy and Resource Utilization are gratefully acknowledged.

## References

- (a) J. R. Long and O. M. Yaghi, *Chem. Soc. Rev.*, 2009, **38**, 1213; (b) T. Uemura, N. Yanai and S. Kitagawa, *Chem. Soc. Rev.*, 2009, **38**, 1228; (c) J. Y. Lee, O. K. Farha, J. Roberts, K. A. Scheidt, S. T. Nguyen and J. T. Hupp, *Chem. Soc. Rev.*, 2009, **38**, 1450; (d) J. R. Li, R. J. Kuppler and H. C. Zhou, *Chem. Soc. Rev.*, 2009, **38**, 1477; (e) L. Ma, C. Abney and W. B. Lin, *Chem. Soc. Rev.*, 2009, **38**, 1248; (f) L. J. Murray, M. Dinca and J. R. Long, *Chem. Soc. Rev.*, 2009, **38**, 1294; (g) O. K. Farha, A. O. Yazaydin, I. Eryazici, C. D. Malliakas, B. G. Hauser, M. G. Kanatzidis, S. T. Nguyen, R. Q. Snurr and J. T. Hupp, *Nat. Chem.* 2010, **2**, 944; (h) B. Yuan, Y. Pan, Y. Li, B. Yin and H. Jiang, *Angew. Chem. Int. Ed.*, 2010, **49**, 4054.
- (a) J. A. Hurd, R. Vaidyanathan, V. Thangadurai, C. I. Ratcliffe, I. L. Moudrakovski and G. K. H. Shimizu, *Nat. Chem.*, 2009, **1**, 705; (b) Y. Kobayashi, B. Jacobs, M. D. Allendorf and J. R. Long, *Chem. Mater.*, 2010, **22**, 4120.
- (a) S. Bureekaew, S. Horike, M. Higuchi, M. Mizuno, T. Kawamura, D. Tanaka, N. Yanai and S. Kitagawa, *Nat. Mater.*, 2009, **8**, 831; (b) N. C. Jeong, B. Samanta, C. Y. Lee, O. K. Farha and J. T. Hupp, *J. Am. Chem. Soc.*, 2012, **134**, 51; (c) T. Yamada, M. Sadakiyo and H. Kitagawa, *J. Am. Chem. Soc.*, 2009, **131**, 3144; (d) M. Sadakiyo, T. Yamada and H. Kitagawa, *J. Am. Chem. Soc.*, 2009, **131**, 9906.
- (a) S. Li, Z. Zhou, Y. Zhang and M. Liu, *Chem. Mater.*, 2005, **17**, 5884; (b) A. Shigematsu, T. Yamada and H. Kitagawa, *J. Am. Chem. Soc.*, 2011, **133**, 2034; (c) M. Sadakiyo, H. Okawa, A. Shigematsu, M. Ohba, T. Yamada and H. Kitagawa, *J. Am. Chem.*

CREATED USING THE RSC ARTICLE TEMPLATE - SEE WWW.RSC.ORG/ELECTRONICFILES FOR FURTHER DETAILS

- Soc., 2012, **134**, 5472; (d) J. M. Taylor, R. K. Mah, I. L. Moudrakovski, C. I. Ratcliffe, R. Vaidhyanathan and G. K. H. Shimizu, *J. Am. Chem. Soc.*, 2010, **132**, 14055.
- 5 (a) G. Férey, F. Millange, M. Morcrette, C. Serre, M. L. Doublet, J. M. Grenèche and J. M. Tarascon, *Angew. Chem. Int. Ed.*, 2007, **46**, 3259; (b) D. Y. Lee, D. V. Shinde, E. K. Kim, W. Lee, I. W. Ohc, N. K. Shrestha, J. K. Lee and S. H. Han, *Microporous Mesoporous Mater.*, 2013, **171**, 53; (c) D. Y. Lee, S. J. Yoon, N. K. Shrestha, S. H. Lee, H. Ahn and S. H. Han, *Microporous Mesoporous Mater.*, 2012, **153**, 163; (d) S. Horike, D. Umeyama and S. Kitagawa, *Acc. Chem. Res.*, 2013, **46**, 2376.
- 6 (a) G. P. Wang, L. Zhang and J. J. Zhang, *Chem. Soc. Rev.*, 2012, **41**, 797; (b) C. X. Guo and C. M. Li, *Energy Environ. Sci.*, 2011, **4**, 4504; (c) P. J. Hall, M. Mirzaeian, S. I. Fletcher, F. B. Sillars, A. J. R. Rennie, G. O. Shitta-Bey, G. Wilson, A. Cruden and R. Carter, *Energy Environ. Sci.*, 2010, **3**, 1238.
- 7 W. Q. Lin, J. D. Leng and M. L. Tong, *Chem. Commun.*, 2012, **48**, 4477.
- 8 (a) H. Liu, S. Ryu, Z. Y. Chen, M. L. Steigerwald, C. Nuckolls and L. E. Brus, *J. Am. Chem. Soc.*, 2009, **131**, 17099; (b) E. Pollak, B. S. Geng, K. J. Jeon, I. T. Lucas, T. J. Richardson, F. Wang and R. Kostecki, *Nano Lett.*, 2010, **10**, 3386; (c) J. A. Robinson, C. P. Puls, N. E. Staley, J. P. Stitt, M. A. Fanton, K. V. Emtsev, T. Seyller and Y. Liu, *Nano Lett.*, 2009, **9**, 964.
- 9 (a) G. M. Sheldrick, *SHELXS 97, Program for Crystal Structure Solution*, University of Göttingen, Göttingen, Germany, 1997; (b) G. M. Sheldrick, *SHELXL 97, Program for Crystal Structure Refinement*, University of Göttingen, Göttingen, Germany, 1997.
- 10 (a) O. D. Friedrichs, M. O'Keeffe and O. M. Yaghi, *Acta Crystallogr.*, 2003, **A59**, 22.; (b) V. A. Blatov, *IUCr CompComm. Newsletter*, 2006, **7**, 4; see also <http://www.topos.ssu.samara.ru>.
- 11 O. D. Friedrichs, M. O'Keeffe and O. M. Yaghi, *Acta Crystallogr. A*, 2003, **59**, 22.
- 12 V. A. Blatov, *IUCr CompComm. Newsl.* 2006, **7**, 4. published online Nov, 2006. See also <http://www.topos.ssu.samara.Ru>.
- 13 A. L. Spek, *Acta Crystallogr., Sect. A: Found. Crystallogr.*, 1990, **46**, C34. The free water molecules were removed before the cited solvent accessible volume was calculated by PLATON.
- 14 B. Tansel, J. Sager, T. Rector, J. Garland, R. F. Strayer, L. F. Levine, M. Roberts, M. Hummerick and J. Bauer, *Sep. Purif. Technol.*, 2006, **51**, 40.
- 15 (a) B. Nepal and S. Das, *Angew. Chem. Int. Ed.*, 2013, **52**, 7224; (b) Y. Gong, H. F. Shi, Z. Hao, W. Hua and J. H. Lin, *Cryst. Growth Des.*, 2014, **14**, 649; (c) Y. Gong, Z. Hao, H. F. Shi, P. G. Jiang, M. M. Zhang and J. H. Lin, *ChemPlusChem*, 2014, **79**, 266; (d) Y. Gong, H. F. Shi, Z. Hao, J. L. Sun and J. H. Lin, *Dalton Trans.* 2013, **42**, 12252; (e) X. L. Gao, Y. Gong, P. Zhang, Y. X. Yang, J. P. Meng, M. M. Zhang, J. L. Yin and J. H. Lin, *CrystEngComm*, 2014, **16**, 8492.
- 16 W. G. Pell and B. E. Conway, *J. Electroanal. Chem.*, 2001, **500**, 121.
- 17 (a) T. D. Bennett and A. K. Cheetham, *Acc. Chem. Res.*, 2014, **47**, 1555; (b) A. J. Graham, A.-M. Banu, T. Düren, A. Greenaway, S. C. McKellar, J. P. S. Mowat, K. Ward, P. A. Wright and S. A. Moggach, *J. Am. Chem. Soc.*, 2014, **136**, 8606; (c) K. W. Chapman, G. J. Halder and P. J. Chupas, *J. Am. Chem. Soc.*, 2009, **131**, 17546; (d) T. D. Bennett, A. L. Goodwin, M. T. Dove, D. A. Keen, M. G. Tucker, E. R. Barney, A. K. Soper, E. G. Bithell, J. C. Tan and A. K. Cheetham, *Phys. Rev. Lett.*, 2010, **104**, 115503; (e) T. D. Bennett, P. Simoncic, S. A. Moggach, F. Gozzo, P. Macchi, D. A. Keen, J. C. Tan and A. K. Cheetham, *Chem. Commun.*, 2011, **47**, 7983; (f) T. D. Bennett, P. J. Saines, D. A. Keen, J. C. Tan and A. K. Cheetham, *Chem. Eur. J.*, 2013, **19**, 7049.
- 18 (a) X. Wang, W. Tian, T. Y. Zhai, C. Y. Zhi, Y. Bando and D. Golberg, *J. Mater. Chem.*, 2012, **22**, 23310; (b) H. Pang, F. Gao, Q. Chen, R. M. Liu and Q. Y. Lu, *Dalton Trans.*, 2012, **41**, 5862; (c) J. P. Cheng, X. Chen, J. S. Wu, F. Liu, X. B. Zhang and V. P. Dravid, *CrystEngComm*, 2012, **14**, 6702; (d) Y. B. Cao, F. L. Yuan, M. S. Yao, J. H. Bang and J. H. Lee, *CrystEngComm*, 2014, **16**, 826; (e) H. Q. Sun, H. M. Ang, M. O. Tadé and S. B. Wang, *J. Mater. Chem. A*, 2013, **1**, 14427; (f) C. R. Zheng, C. B. Cao, Z. Ali and J. H. Hou, *J. Mater. Chem. A*, 2014, **2**, 16467; (g) G. X. Wang, X. P. Shen, J. Horvat, B. Wang, H. Liu, D. Wexler and J. Yao, *J. Phys. Chem. C*, 2009, **113**, 4357.
- 19 (a) M. Hunsom, *Spectrosc. Prop. Inorg. Organomet. Compd.*, 2012, **42**, 196; (b) S. A. Mamuru, K. I. Ozoemena, T. Fukuda and N. Kobayashi, *J. Mater. Chem.*, 2010, **20**, 10705; (c) S. Ghosh, R. K. Sahu and C. R. Raj, *J. Mater. Chem.*, 2011, **21**, 11973.

